HHS Public Access

Author manuscript

*Cell Rep*. Author manuscript; available in PMC 2015 September 01.

Published in final edited form as:

*Cell Rep*. 2014 October 9; 9(1): 180–192. doi:10.1016/j.celrep.2014.08.074.

# Dnase2a deficiency uncovers lysosomal clearance of damaged nuclear DNA via autophagy

**Yuk Yuen Lan**[1,2,3,7], **Diana Londoño**[1,2,6,7], **Richard Bouley**[4], **Michael S. Rooney**[5], and **Nir Hacohen**[1,2,3,*]

[1]Center for Immunology and Inflammatory Diseases, Massachusetts General Hospital, 149 13th Street, Charlestown, MA 02129, USA

[2]Broad Institute, 415 Main Street, Cambridge, MA 02142, USA

[3]Department of Medicine, Harvard Medical School, Boston, MA 02115, USA

[4]Center for Systems Biology, Program in Membrane Biology and Nephrology Division, Massachusetts General Hospital, 185 Cambridge Street, Boston, MA 02114, USA

[5]Harvard/MIT Division of Health Sciences and Technology, Cambridge, Massachusetts 02139, USA

## Summary

Deficiencies in DNA degrading nucleases lead to accumulation of self DNA and induction of autoimmunity in mice and in monogenic and polygenic human diseases. However, the sources of DNA and the mechanisms that trigger immunity remain unclear. We analyzed mice deficient for the lysosomal nuclease, *Dnase2a*, and observed elevated levels of undegraded DNA in both phagocytic and non-phagocytic cells. In non-phagocytic cells, the excess DNA originated from damaged DNA in the nucleus based on co-localization studies, live cell imaging and exacerbation by DNA-damaging agents. Removal of damaged DNA by Dnase2a required nuclear export and autophagy-mediated delivery of the DNA to lysosomes. Finally, DNA was found to accumulate in *Dnase2a*$^{-/-}$ or autophagy-deficient cells and induce inflammation via the *Sting* cytosolic DNA-sensing pathway. Our results reveal a cell-autonomous process for removal of damaged nuclear DNA with implications for conditions with elevated DNA damage, such as inflammation, cancer and chemotherapy.

*Correspondence: nhacohen@partners.org.

[6]Present address: Department of Neurology, The Illinois Neurologic Institute, 530 NE Glen Oak Avenue, University of Illinois College of Medicine, Peoria, IL 61637, USA

[7]These authors are co-first authors

The authors declare no conflict of interest.

YYL and NH conceived the project, designed experimental strategies and wrote the manuscript. DL performed, analyzed and quantified histological and fluorescence imaging. RB performed the time-lapse imaging experiments. MSR performed the computational analysis of DNA deep sequencing and assisted in statistics. All authors contributed to interpretation and discussion. YYL performed all other experiments and NH supervised the work.

## Introduction

Mammalian cells express numerous nucleic sensors that detect and induce responses to invading viruses and other microbes (Barber, 2011; Paludan and Bowie, 2013). While this suite of sensors can also recognize self DNA and RNA, several mechanisms are in place to avoid such innate immune responses to self. First, a subset of the RNA and DNA sensors -- TLR3, 7, 8 and 9 -- are localized to endosomal compartments that appear to be spatially segregated from self nucleic acids (Ishii and Akira, 2006; Stetson and Medzhitov, 2006). For example, when TLR9 is engineered to localize on the surface of cells, it recognizes circulating DNA and induces inflammation (Barton et al., 2006). Second, self nucleic acids may have modifications that render them undetectable to some sensors (Iwasaki, 2012). Finally, nucleases clear cells of excess nucleic acids that might otherwise activate sensors. Evidence for this last mechanism is abundant, as mutations in DNases and RNases lead to autoimmunity in mouse models and in human monogenic and polygenic diseases.

Specifically, mutations in *Dnase1* (Napirei et al., 2000; Yasutomo et al., 2001), *Dnase2* (Kawane et al., 2006; Kawane et al., 2010), *Dnase3/Trex1* (Crow et al., 2006; Lee-Kirsch et al., 2007; Morita et al., 2004), enable self DNA originating from apoptotic cells (Yoshida et al., 2005) or retroelements (Stetson et al., 2008) to accumulate and results in autoimmune diseases, including systemic lupus erythematosus and Aicardi-Goutiéres syndrome in humans (Crow et al., 2006; Lee-Kirsch et al., 2007; Yasutomo et al., 2001), and autoimmune arthritis (Kawane et al., 2006; Kawane et al., 2010), nephritis (Gall et al., 2012) and myocarditis (Morita et al., 2004) in mice. Studies of the *Trex1/Dnase3* gene that degrades DNA (Chowdhury et al., 2006; Mazur and Perrino, 2001) clearly demonstrate the consequences of cells over-reacting to self DNA. *Trex1*−/− mice were shown to develop a lethal autoimmune cardiomyopathy (Morita et al., 2004) with associated accumulation of single-stranded DNA produced in S phase (Yang et al., 2007); subsequent studies implicated undegraded retroelements as a source of immunostimulatory DNA (Stetson et al., 2008) and demonstrated the importance of the *Sting* DNA-sensing pathway in triggering inflammation and autoimmunity (Gall et al., 2012).

Another example is *Dnase2a*, a ubiquitously expressed lysosomal DNA endonuclease that degrades DNA to oligonucleotides and nucleotides (Evans and Aguilera, 2003). *Dnase2a*$^{-/-}$ mice spontaneously produce high levels of Type I IFNs and show embryonic lethality that is rescued by removing the IFN receptor (Yoshida et al., 2005). Conditional ablation of *Dnase2a* in adult mice leads to production of immune cytokines (e.g. TNF-α, IL-6, CXCL10, IL-1β and Type I IFNs), autoantibodies (rheumatoid factor and anti-dsDNA) and development of chronic polyarthritis that resembles human rheumatoid arthritis (Kawane et al., 2006). Consistent with the role of lysosomes in recycling materials ingested via endocytosis, undigested DNA (partly derived from discarded erythrocyte nuclei) was found in fetal liver macrophages in *Dnase2a* knockout mice (Kawane et al., 2001; Krieser et al., 2002).

These two models of DNase deficiency demonstrate that defective degradation of nucleic acids can activate autoimmune responses, and yet the source and mechanism of clearance of DNA remain unclear. We focused on the *Dnase2a*-knockout as a genetic model to dissect

the source and sub-cellular localization of DNA and the mechanisms that trigger immunity, and observed unexpected accumulation of nuclear DNA outside the nucleus. Further experiments led us to define a mechanism by which lysosomal *Dnase2a* clears damaged nuclear DNA via autophagy.

## Results

### DNA accumulates in phagocytic and non-phagocytic *Dnase2a*-deficient cells

We hypothesized that phagocytic cells likely accumulate the highest levels of DNA in *Dnase2a*-deficient animals based on their ability to ingest erythrocyte nuclei and apoptotic cells (Krieser et al., 2002; Yoshida et al., 2005). Consistent with the hypothesis, we detected excessive DNA content in professional phagocytes (using propidium iodine [PI] and other DNA dyes such as Ruby and Hoechst), including bone marrow-derived dendritic cells (BMDCs) and splenic DCs from *Dnase2a*$^{-/-}$ mice (Figure 1A), as well as primary BMDCs silenced for *Dnase2* by stably-expressed shRNAs. To determine the distribution of DNA in these mice, we stained tissue sections with DAPI and observed higher levels of DNA in cells of joints, kidney and liver of knockout (*Dnase2a*$^{-/-}$) relative to wild-type (*Dnase2a*$^{+/+}$) mice (Figure 1B). Concomitant with the heightened inflammation previously observed in *Dnase2a*$^{-/-}$ mice, we detected elevated levels of inflammatory genes (the IFN-inducible chemokine, *Cxcl10* and the cytokines, *Il6* and *Tnfα*) in all cell types (B and T cells, DCs, macrophages) of the spleen from knockout mice relative to control littermates. This global activation could occur as a result of independent, autonomous events in each cell type or a cascade of inflammation initiated by a small number of cells.

We were surprised to observe increased DNA levels in non-phagocytic lymphocytes (primary T and B cells, Figure 1C; with the small fraction of genomic DNA representing a significant absolute level of DNA) and non-immune cells, including primary lung and skin fibroblasts, long-term cultured mouse lung fibroblasts (MLFs), in knockout versus wild-type mice; and *p53*$^{-/-}$ mouse embryonic fibroblasts (MEFs) silenced with *Dnase2a*-targeting shRNAs (Figure S1A). To exclude the possibility that *Dnase2a*$^{-/-}$ cells are more often in S phase (>2n DNA) relative to wild-type cells, we synchronized non-phagocytic MLFs of both genotypes and observed a similar increase in DNA by PI staining (Figure 1D; Ruby staining showed same result). We also confirmed the higher DNA content in *Dnase2a*$^{-/-}$ cells with independent measurements, including UV absorbance of purified genomic DNA (Figure 1E), which correlated well with mean intensity of dye-stained cells by flow cytometry (Figure S1B). These results imply that *Dnase2a* is essential for preventing the accumulation of DNA, not only as expected in phagocytic cells, but also in non-phagocytic cells.

### Damaged DNA is found outside the nucleus of *Dnase2a*-deficient cells

We suspected that the excess DNA could be derived from an intracellular source. To pinpoint the location of accumulated DNA within *Dnase2a*-deficient cells, we stained MLFs with anti-dsDNA antibodies. We observed small and large DNA aggregates at peri-nuclear regions (Figure 2A, untreated), and interestingly, adjacent to condensed chromosomes of dividing cells (Figure S2A, untreated). We thus hypothesized that damaged chromosomal

DNA would need to be discarded during replication or DNA damage and repair and exported from the nucleus for degradation by Dnase2a.

To visualize DNA fragments generated by damage or repair, we stained tissues and cultured cells for phosphorylated histone 2AX (γ-H2AX), an established marker of double-stranded DNA breaks (DSBs). *In vivo* staining of γ-H2AX was dramatically elevated in the kidneys of *Dnase2a*-deficient relative to wild-type mice (Figure 2B), and similarly *in vitro* in *Dnase2a*-deficient MLFs (Figure 2C, untreated), suggesting that damaged DNA accumulates to high levels in the absence of *Dnase2a* in the steady state. We also noted that there was increased nuclear DNA and γ-H2AX signal in the nucleus of *Dnase2a*$^{-/-}$ MLFs (Figure 2A, 2C, 2D). Whether excess extra-nuclear DNA may hinder the export of damaged nuclear DNA and thus promote DNA damage in the nucleus is an open question.

To increase the burden of endogenous damaged DNA, we treated cells or mice with cytarabine (Ara-C), a nucleoside analog that causes replication stalls, and observed even higher levels of extra-nuclear DNA in cells (Figures 2A, treated) while cell viability remained high (Figure S2B). In addition, *p53*$^{-/-}$ MEFs, which have defects in the regulation of DNA repair, showed clear dose-responsive DNA accumulation to Ara-C by flow cytometry and immunostaining (Figure S2C, S2D). Two different anti-dsDNA antibodies (sc-58749, DNA11-M) and serum from NZB/NZW lupus mice gave similar staining results. DAPI staining also showed similar patterns but required acetone fixation and did not reveal the small DNA speckles in the cytosol (Figure S2E). Pre-incubation with DNA, including salmon DNA, calf thymus DNA and IFN-stimulatory DNA (ISD) and digest with DNase I confirmed the specificity of the anti-dsDNA antibody (Figure S2F, S2G). We note that MLFs with excessive levels of damaged DNA did not detectably transfer their DNA to cells with normal levels of DNA after 24 hours of co-culture, indicating that the observed extra-nuclear DNA aggregates were not derived from extra-cellular sources (Figure S2H).

Importantly, the γ-H2AX signal, which was higher in *Dnase2a*$^{-/-}$ cells after Ara-C treatment (Figure 2C, treated), co-localized with dsDNA both at peri-nuclear buds and cytosolic speckles (Figure 2D). Furthermore, *in vivo* treatment of Ara-C aggravated joint swelling in *Dnase2a*$^{-/-}$ mice suggesting that damaged DNA could exacerbate arthritis in this model (Figure 2E, we used younger animals at 4 months of age before development of arthritis). Thus, the extra-nuclear DNA accumulating in *Dnase2a*-deficient cells — spontaneously or induced by DNA-damaging agents — appears to consist of damaged dsDNA fragments.

## Accumulated DNA originates in the nucleus

Supporting the nuclear origin of accumulated DNA, three major spatial patterns of extra-nuclear DNA were observed by confocal microscopy (Figure 3A, relative frequencies in right panel): (1) nuclear buds that appear continuous with the nucleus (found in *Dnase2a*$^{-/-}$ but rarely in wild-type cells); (2) cytosolic speckles that fan out from the nucleus (most prominent upon Ara-C treatment); (3) large extra-nuclear aggregates that are likely to be detached nuclear buds based on their shape, size and proximity to the nucleus (mostly in Ara-C treated cells). High-resolution fluorescence and electron microscopy staining for dsDNA further confirmed the presence of DNA buds and speckles (emanating at specific

points) in close apposition with the nucleus (Figure 3B). Buds and speckles were often encircled by or co-localized with the nucleoporin protein, NUP98, a docking site for transport at the nuclear pore complex and marks the nuclear envelope (Figure 3C). When the fate of newly synthesized nuclear DNA was tracked with BrdU, we observed comparable patterns of peri-nuclear buds and cytosolic speckles emanating from the nucleus (Figure 3D), indicating that replicated DNA contributed to extra-nuclear DNA.

We tested the potential of mitochondria to contribute excess DNA, and found that MitoTracker signal (Figure S3A) and PCR-based quantitation of mitochondrial DNA (Figure S3B) was not significantly different between *Dnase2a*$^{+/+}$ and *Dnase2a*$^{-/-}$ cells. Only a minor fraction of extra-nuclear DNA co-localized with mitochondria by immunofluorescence (Figure S3C). To further exclude mitochondria as a source of DNA, we used aphidicolin to inhibit nuclear but not mitochondrial replication (Ikegami et al., 1978), and observed abrogation of the cytosolic DNA accumulation in the presence of Ara-C (Figure S3D). The observations of dsDNA accumulation along with experiments excluding mitochondria indicate that the nucleus is the major source of accumulated DNA in *Dnase2a* knockout and Ara-C treated cells.

## DNA is exported from nucleus

To study the spatial and temporal dynamics of excess DNA, we infected wild-type and *Dnase2a*$^{-/-}$ MLFs with a retrovirus carrying GFP-H2B. While DNA dyes (e.g. Hoechst, Ruby) induce photo-toxicity and limit their use for live capture, histone proteins are known to associate tightly with DNA and have been used as surrogate markers for DNA (Kanda et al., 1998). We confirmed the co-localization of GFP-H2B with dsDNA in the cytosol by immunofluorescence (Figure S3E). Time-lapse live imaging of Ara-C treated cells with a spinning disc confocal microscope revealed several steps of the nuclear DNA export process, including nuclear DNA bud formation and detachment of nuclear DNA from the nucleus into the cytosol (through unusual thread-like structures that are first connected to the nucleus and then fragment in the cytosol) after 2–8 h of Ara-C treatment (Figure 3E and Video 1, Video 2). These live observations demonstrate that endogenous DNA moves out of the nucleus when cells are under genotoxic stress.

## Accumulated DNA induces inflammation

The abnormally high level of damaged DNA outside the nucleus has the risk of activating innate immune DNA-sensing pathways that induce cytokine and chemokines. Indeed, Ara-C as well as topoisomerase inhibitors (doxorubicin and etoposide that act through independent mechanisms) not only caused a rise in DNA levels but also upregulated chemokine and cytokine gene expression (including *Cxcl10*, *Ifnb*, *Il6*, *Tnfa*) in a dose-dependent manner in *p53*$^{-/-}$ MEFs (unpublished data). In MLFs, we found that the upregulation of *Cxcl10* expression as a result of Ara-C treatment was most pronounced when *Dnase2a* was absent (Figure 4A). Confirming that the excessive DNA and *Cxcl10* levels observed in *Dnase2a*$^{-/-}$ MLFs were indeed due to lack of degradation by Dnase2a, we successfully rescued the inflammatory and extra-nuclear DNA phenotypes with inducible *Dnase2a* expression (*Cxcl10*, Figure 4B; dsDNA, Figure 4C). Furthermore, the known adaptor *Sting/Tmem173* and mediator *Tbk1* of the cytosolic DNA-sensing pathway, were expressed at higher levels

in knockout compared to wild-type MLFs (Figure S4A), and siRNA-mediated silencing of either mediator abolished the heightened immune activation observed in *Dnase2a*-deficient and Ara-C-treated cells (Figure 4D), consistent with loss of arthritis in *Dnase2a*$^{-/-}$ *Sting*$^{-/-}$ mice (Ahn et al., 2012). Finally, corroborating the nuclear origin of the accumulated DNA, inhibition of nuclear export by leptomycin B (LMB) almost completely abolished cytokine production (Figure 4E) in MLFs, while ISD-induced *Cxcl10* expression was only partially reduced (Figure S4B). Thus, exported nuclear DNA that accumulates as a result of a *Dnase2a* deficiency or induction of DNA damage engages a *Sting*-dependent cytosolic nucleic acid sensing pathway to induce inflammation.

## DNA localizes with autophagosomes and lysosomes

Given that Dnase2a co-localizes with DNA in a LAMP1$^{+}$ compartment, a key question is how extra-nuclear DNA is transported to the lysosome for degradation by Dnase2a. We considered the possibility that autophagy, a major mechanism for recycling of cytosolic cargo, would deliver the excess DNA to lysosomes. Indeed, canonical autophagy genes, including *Atg5*, *Atg7*, *Beclin1*, were significantly upregulated in *Dnase2a*-deficient MLFs compared with wild-type cells (Figure 5A). The autophagosomal marker LC3-II and the lysosomal protein LAMP1 were also elevated in *Dnase2a*$^{-/-}$ and Ara-C-treated MLFs (Figures 5B, 5C) and in *Dnase2a*$^{-/-}$ kidneys (Figure 5D) compared with those in wild-type. LC3 formed the typical punctate cytosolic pattern found during active autophagy.

To further visualize the overlap of autophagosomes and lysosomes with cytosolic DNA in the DNA degradation process, we used antibodies against LC3 and LAMP1 to study their co-localization with dsDNA. In Ara-C-treated wild-type cells, excess DNA co-localized with LC3 and LAMP1, likely reflecting autophagosome-lysosome fusion and the depositing of nuclear DNA into the lysosomal degradation pathway (Figure 5E, top, seen also in untreated wild-type cells [left], but this is a rare event). Confirming our findings, we note that the nucleo-cytoplasmic distribution of LC3 that we observe has been reported (Drake et al., 2010) and that GFP-LC3 showed similar intensity, punctate pattern and co-localization with DNA (Figure S5A, S5B). In contrast, in *Dnase2a*-deficient MLFs, DNA aggregates did not localize with LAMP1, yet remained localized with LC3 (Figure 5E, bottom; also Figure S5C showing enlarged nuclear buds, and reduced DNA/LAMP1 and LC3/LAMP1 co-localization in Figure 5F). We suspect that aborted fusion may be a quality control mechanism for avoiding lysosomes that lack degradation enzymes, and results in accumulation of autophagosomes similar to what is observed in lysosomal storage disorders lacking hydrolases (Settembre et al., 2008).

## Requirement for autophagy and lysosomes in autonomous DNA removal

Based on these data, we predicted that a defect in autophagy, like a deficiency in *Dnase2a*, would lead to elevated levels of DNA in the cell. We found that *Atg5*$^{-/-}$ MEFs amassed higher levels of DNA (Figure 6A, Ruby staining; Figure 6B, anti-dsDNA immunostaining), with elevated cytosolic speckles and aggregates (Figure 6C), but lacked co-localization of DNA with lysosomes (Figure 6D). Consistent with a role for autophagy in removing immunostimulatory DNA that could engage cytosolic DNA sensing pathways, basal

increase of DNA levels in *Atg5*$^{-/-}$ MEFs was sufficient to mount an immune response, while Ara-C treatment heightened the level of cytokine expression (Figure 6E).

To test the role of the lysosome in DNA clearance, we blocked vesicular fusion to lysosomes using bafilomycin A1 (which inhibits V-ATPases and lysosomal acidification) and found enhanced accumulation of extra-nuclear DNA in wild-type MLFs treated with Ara-C (Figure S6). In contrast, the autophagy inducer rapamycin reduced the levels of cytosolic DNA in knockout cells (Figure S6). These data reveal a nuclear-to-autophagosome-to-lysosome transport pathway that targets nuclear DNA for degradation and is upregulated in the context of DNA damage. We note that silencing *Atg5* resulted in elevated DNA levels and *Cxcl10* expression that were beyond those observed in the *Dnase2a*$^{-/-}$ cells (Figure 6F). The synergistic phenotype of *Atg5*/*Dnase2a* deficient cells suggests the existence of additional autophagy-dependent mechanisms of DNA clearance beyond *Dnase2a*. Importantly, double-knockdown of *Atg5* with *Sting* or *Tbk1* eliminated the immune response (Figure 6F), consistent with a role for STING in sensing damaged DNA (and its observed association with autophagosomes in the presence of DNA (Saitoh et al., 2009; Watson et al., 2012)).

## Discussion

An important question in immunology is whether self DNA can trigger the normal viral sensing pathways, and if it does, what is the source of self DNA. We addressed these questions using *Dnase2a*$^{-/-}$ mice that develop arthritis and accumulate self DNA. Previous studies show that *Dnase2a* degrades DNA from ingested apoptotic cells (Kawane et al., 2001), and can even degrade entire genomes autonomously when cells die during development in fly (Bass et al., 2009). In contrast, our study focuses on an unexpected process by which lysosomal *Dnase2a* autonomously degrades damaged DNA that is exported from the nucleus in living cells (Schematic in Figure S7).

In our study, we provide multiple lines of evidence that excess DNA in *Dnase2a*-deficient cells consists of exported nuclear DNA fragments. An important question is why the presence of extranuclear DNA has not been reported more regularly. We hypothesize that Dnase2a removes the exported DNA rapidly – before it can be visualized – analogous to the historical difficulties in observing apoptotic cells in animals due to their immediate removal by phagocytic cells. The observation of increased buds at the nuclear envelope in Dnase2a-deficient cells may thus indicate a higher rate of damaged DNA generation than removal. Nevertheless, other studies have detected DNA fragments arising from replication in budding yeast (Sogo et al., 2002) and fly (Blumenthal and Clark, 1977), over represented dsDNA fragments from chromosomes as free dsDNA molecules in human cells during S phase (Gomez and Antequera, 2008), and release of short DNA fragments into the cytosol prompted by physical (Kawashima et al., 2011) or radiation-induced injury (Pang et al., 2011). Interestingly, unrepaired or irreparable DNA has been found to re-localize to the nuclear periphery (Nagai et al., 2008; Oza et al., 2009), suggesting that it may be segregated from replicating DNA for clearance. These studies along with those in *Trex1*$^{-/-}$ cells (Stetson et al., 2008; Yang et al., 2007) -- are consistent with our findings.

Testing the *in vivo* impact of autonomous damaged DNA on inflammation is not feasible at this time because we cannot eliminate the effects of extra-cellular DNA in animals. However, prior studies of DNA repair gene KO models, in which generation of damaged DNA is elevated, are consistent with our cellular model. For example, $ATM^{-/-}$ cells accumulate cytoplasmic double-strand telomeric DNA in mouse and human cells (Hande et al., 2001), and $Atm^{-/-}$ and $p53^{-/-}$ MEFs show increased basal interferon-stimulated genes (ISGS) (Sugihara et al., 2011). Furthermore, p53 has been strongly implicated in autoimmune suppression and its over-expression limits arthritis development through STAT-mediated regulation (Park et al., 2013). A more detailed analysis of the excess DNA in *Dnase2*$^{-/-}$ cells, will be informative for tracing the chromosomal origin of the observed damaged DNA fragments (e.g. to mutation-prone common fragile sites (Ozeri-Galai et al., 2012), or early replication fragile sites (Barlow et al., 2013), regions of increased synthesis at re-replication sites (Green et al., 2010) or nucleosome-free gaps (Gomez and Antequera, 2008)).

We also observed that extranuclear DNA localizes in small speckles and large buds/aggregates and is often associated with the nuclear envelope. Furthermore, these structures co-localized with the autophagy machinery that is required for their clearance. These steps resemble the recently described phenomenon of nucleophagy (by which autophagy removes pieces of the nucleus (Mijaljica et al., 2010)), which is best described in yeast where piecemeal microautophagy of the nucleus pinches and degrades nuclear components in rapidly dividing cells, a process often induced by nutrient deprivation or rapamycin treatment (Krick et al., 2008; Roberts et al., 2003). Other examples include whole nuclei removal in fungi (Shoji et al., 2010) as well as micronuclei in human cancer cells (Rello-Varona et al., 2012). In humans, nuclear laminopathies (caused by mutations in *Lmna*, encoding lamin A and C that form the structural support of the nucleus) and envelopathies (caused by mutations in *emerin*, a trans-membrane protein on the inner nuclear membrane binding to lamin) (Dauer and Worman, 2009) show resemblance to our cellular observations —in cells with mutations in lamin A, giant peri-nuclear autophagosomes or autolysosomes containing DNA form apparently because of loss of integrity in the nuclear structure and extrusion of damaged nuclei into the cytoplasm (Park et al., 2009). Nucleophagy has not been dissected in detail in mammals and its exact relationship to our findings is not known (Mijaljica et al., 2010). Finally, a recent study reports that γ-H2AX positive cytosolic chromatin fragments are processed by autophagy in senescent cells (Ivanov et al., 2013).

Our observation that undigested DNA is not present in lysosomes of Dnase2a KO cells indicates an additional regulatory step controlling the trafficking (Cai et al., 2007) and fusion of autophagosomes to lysosomes (e.g., analogous to lack of accumulated products in lysosomes in the absence of lysosomal hydrolases (Settembre et al., 2008). More importantly, how autophagy and the DNA sensing pathway interact requires further studies. A recent report that finds increased radio-sensitivity of ATG5 or BCN1-depleted cells and reduced $ATG5^{-/-}$ tumor growth after irradiation (Ko et al., 2014) may be related to our finding that autophagy affects trafficking of damaged DNA. Furthermore, the ATG5 locus has been shown to affect susceptibility to lupus (Delgado-Vega et al., 2010; Graham et al.,

2009; Kaiser and Criswell, 2010), suggesting that perhaps the risk allele causes patient cells to amass DNA and induce excessive inflammation.

Prior studies have shown that ATM and NF-κB are critical in the induction of inflammation by DNA damage (Hinz et al., 2010; Yang et al., 2011) and that damaged DNA appears to stimulate the Type I IFN response (Brzostek-Racine et al., 2011). Here, we add to these mechanistic studies by showing a requirement for *Sting* and *Tbk1* in the induction of inflammation in response to excess damaged DNA (consistent with *Dnase2a*$^{-/-}$*Sting*$^{-/-}$ mice not developing arthritis (Ahn et al., 2012)). Surprisingly, recent studies have found that DNA damage response (DDR) components Mre11 (Kondo et al., 2013), DNA-PK (Ferguson et al., 2012) and Ku70 (Zhang et al., 2011) (as well extra chromosomal histone H2B (Kobiyama et al., 2010)) are also required for induction of the cytosolic DNA-sensing pathway. Interestingly, some of the DNA repair proteins have also been found to be cleared by autophagy after DSB repair (Robert et al., 2011), suggesting that DDR proteins may bind the exported DNA fragments we observe, and perhaps play a role in their stabilization, transport, and immune sensing. Together, these results point to an interesting yet poorly understood pathway that links damaged DNA, DNA repair proteins and the innate immune response.

Why are there many nucleases involved in clearance of self DNA? It is likely that they specialize by targeting particular substrates within different subcellular compartments. For example, *Dnase2a* and *Trex1* are both critical nucleases that prevent cells from accumulating self DNA and triggering autoimmunity. Although deficiencies in either nuclease leads to *Sting*-dependent autoimmunity (Ahn et al., 2012; Gall et al., 2012), Trex1 associates with cytosolic face of the ER and targets ssDNA while Dnase2a sits in the lysosome and degrades dsDNA. Interestingly, a recent study observed upregulation of lysosomes in *Trex1*$^{-/-}$ cells (Hasan et al., 2013), suggesting that excess DNA may be triggering autophagy/Dnase2a-mediated clearance to compensate for lack of *Trex1*. Trex1 is able to degrade retroelement ssDNA (Stetson et al., 2008); however, consistent with the role of Dnase2a in degrading dsDNA, our preliminary deep sequencing of cytosolic DNA from *Dnase2*$^{-/-}$ cells did not show enrichment of retroelements (e.g. SINE, LINE, LTR sequences). Thus, while both nucleases are equally important for homeostasis, their DNA substrates, localization and impact on disease appear to be distinct.

Finally, some of our findings may help explain the therapeutic effect of DNA-damaging agents in cancer. Such agents have been found to induce anti-tumor immunity (Galluzzi et al., 2012), and in other studies to activate the IFNβ-Stat1-ISG axis (Brzostek-Racine et al., 2011; Novakova et al., 2010). Our results suggest that the damaged DNA induced by these treatments would be exported from the nucleus and engage innate immune sensing pathways that could modulate tumor immunity.

## Experimental Procedures

### Mice

*Dnase2a*$^{flox/-}$ and *Mx1-Cre* mice, a gift from Dr. Shigekazu Nagata (Kyoto University, Japan) were bred and genotyped to obtain conditional *Dnase2a*$^{flox/-}$ *Mx1-Cre* mice. Wild-

type littermates with matched age and sex were selected as controls. Both genotypes were injected *i.p.* with 1.5 μg/weight (g) of poly I:C 3x every other day at 12–16 weeks of age to induce deletion of *Dnase2a* as described (Kawane et al., 2006). Mice were housed in a specific pathogen-free facility at MGH, and protocols were approved by MGH SRAC in accordance with the institutional animal ethics guidelines.

### Cell isolation and culture

Lungs of mice were finely cut and digested with 1 mg/ml collagenase D (Roche) and 20 U/ml DNase1 (Roche). Mouse lung fibroblasts were cultured in DMEM, 15% FBS, 1% P/S, NEAA, sodium pyruvate, Hepes and L-glutamate. Spleens were homogenized and digested the same way, filtered through 70 μm cell strainer and treated with red blood cell lysing buffer (Sigma). B, T and dendritic cells were enriched by antibody-conjugated beads (Miltenyi). Mouse embryonic fibroblasts (*p53*-deficient) were sub-cultured (1:20) in DMEM with 10% FBS and 1% P/S.

### DNA content

Live cells were stained with Vybrant® DyeCycle™ Ruby stain (Invitrogen) and fixed cells with PI at 50 μg/ml, 40 min, 37°C. Genomic DNA was isolated using GenElute™ mammalian genomic DNA miniprep kit (Sigma-Aldrich) for measurement by UV spectrophotometry.

### Ara-C experiment

For induction of DNA damage, we used 24 h *in vitro* treatment of Ara-C at 10 μM or as indicated (Sigma-Aldrich). Sex-matched 10–12 weeks old wild-type or *Dnase2a*$^{-/-}$ mice were untreated or injected *i.p.* with 3 consecutive doses of 15 μg/weight (g) Ara-C every 2 days. Weight and ankle thickness was measured at weeks 1, 2, 3, 4, 6, 8 and compared to baseline at week 0. At the end of week 8, mice were euthanized and tissues dissected for H&E and immunohistochemistry.

### *Dnase2a* rescue

*Dnase2a* ORF was cloned into a pCW57d-P2AR lentiviral Tet-on vector with puromycin resistance (The RNAi Consortium, Broad Institute). Plasmid DNA was purified and transfected into 293 cells for packaging of lentiviruses. *Dnase2a*$^{-/-}$ MLFs were infected with *Dnase2a* ORF or control eGFP virus, puromycin-selected (10 μg/ml) and seeded in 24-well plates for doxycycline induction (3 μg/ml, 24–48 h). *Dnase2a* expression was confirmed by RT-qPCR.

### Knockdown experiments

Cells were infected with puromycin-resistant lentiviral vector encoding shRNAs to *Dnase2a*, *Atg5* or control, or transfected with 150 nM of siGENOME pool siRNA (Dharmacon) targeting *Atg5*, *Tbk1*, *Sting*, or negative control, using Lipofectamine™ RNAiMAX (Life Technologies). Knockdown efficiency was confirmed by RT-qPCR.

### Immunofluorescence cell staining

We fixed cells with 4% PFA, permeabilized, blocked and stained with antibodies against: dsDNA (Santa Cruz), γ-H2AX, NUP98, (Cell Signaling), LC3 (Novus Biologicals), biotin-LAMP1 and BrdU (BioLegend), followed by fluorescent secondary antibodies or streptavidin. Images were captured using a Nikon eclipse ME600 fluorescence or Zeiss LMS510 confocal microscope, processed with NIS-elements AR 2–30 or Carl Zeiss microimaging software, and analyzed with ImageJ across 5–20 random fields from at least 2 different experiments.

### Live-cell imaging

Live-cell imaging was performed on MLFs grown on a glass bottom tissue culture dishes (FluroDish, World Precision Instruments) to reach 60–80% confluence. Cell images were visualized using a spinning-disk confocal system (Ultraview confocal scanner, Perkin Elmer) equipped with a Nikon Eclipse TE2000-U microscope and an environmental chamber (37°C, 5% $CO_2$) (Solent Scientific). Images were acquired with a plan APO TIRF Nikon oil immersion objective (60x 1.45) every 3–5 min for 2–8 h using Z code stack. The images were processed with Volocity software (Volocity 6, PerkinElmer Inc).

### Statistical analyses

All statistical analyses were performed using GraphPad PRISM 4 (GraphPad Software). All values were expressed as mean±sem. Samples were analyzed using Student's t-test or as indicated, with * denoting $p < 0.05$, **$p < 0.01$, and ***$p < 0.001$.

## Supplementary Material

Refer to Web version on PubMed Central for supplementary material.

## Acknowledgments

We thank Shigekazu Nagata and Kohki Kawane (Kyoto University, Japan) for *Dnase2a*-deficient mice; Ramnik Xavier for *Atg5*$^{-/-}$ MEFs; Francesco Marangoni, Flavia Castelino and Norihiko Sakai for technical advice; Weibo Li, Matthew Roy and Mark Lee for technical help and reagents. We thank Cyrus Vaziri for advice on DNA damaging agents. We thank Raquel Deering, Tom Eisenhaure, Marko Jovanovic, Dan-Avi Landau, Mark Lee, Karolina Maciag, Will Pendergraft and Chloe Villani of the Hacohen laboratory, for comments on the manuscript. We appreciate assistance of Thomas J. Diefenbach with confocal microscopy at the Ragon Institute Imaging Core; Ravi Mylvaganam with flow sorting at the Department of Pathology; Mary McKee with electron microscopy at the Center for Systems Biology/Program in Membrane Biology, (supported by NIH DK43351 and DK57521); and the CCM staff for laboratory animal care. YYL thanks M. Amin Arnaout (T32 DK007540-22) and Andrew D. Luster (T32 AI060548-04, T32 AI060548-05) for training grant support. This work was supported by the NIH Director's New Innovator Award (DP2 OD002230) and the MGH Research Scholars Program to NH.

## References

Ahn J, Gutman D, Saijo S, Barber GN. STING manifests self DNA-dependent inflammatory disease. Proc Natl Acad Sci U S A. 2012; 109:19386–19391. [PubMed: 23132945]

Barber GN. Cytoplasmic DNA innate immune pathways. Immunol Rev. 2011; 243:99–108. [PubMed: 21884170]

Barlow JH, Faryabi RB, Callen E, Wong N, Malhowski A, Chen HT, Gutierrez-Cruz G, Sun HW, McKinnon P, Wright G, et al. Identification of early replicating fragile sites that contribute to genome instability. Cell. 2013; 152:620–632. [PubMed: 23352430]

Barton GM, Kagan JC, Medzhitov R. Intracellular localization of Toll-like receptor 9 prevents recognition of self DNA but facilitates access to viral DNA. Nat Immunol. 2006; 7:49–56. [PubMed: 16341217]

Bass BP, Tanner EA, Mateos San Martin D, Blute T, Kinser RD, Dolph PJ, McCall K. Cell-autonomous requirement for DNaseII in nonapoptotic cell death. Cell Death Differ. 2009; 16:1362–1371. [PubMed: 19557011]

Blumenthal AB, Clark EJ. Discrete sizes of replication intermediates in Drosophila cells. Cell. 1977; 12:183–189. [PubMed: 902313]

Brzostek-Racine S, Gordon C, Van Scoy S, Reich NC. The DNA damage response induces IFN. J Immunol. 2011; 187:5336–5345. [PubMed: 22013119]

Cai H, Reinisch K, Ferro-Novick S. Coats, tethers, Rabs, and SNAREs work together to mediate the intracellular destination of a transport vesicle. Dev Cell. 2007; 12:671–682. [PubMed: 17488620]

Chowdhury D, Beresford PJ, Zhu P, Zhang D, Sung JS, Demple B, Perrino FW, Lieberman J. The exonuclease TREX1 is in the SET complex and acts in concert with NM23-H1 to degrade DNA during granzyme A-mediated cell death. Mol Cell. 2006; 23:133–142. [PubMed: 16818237]

Crow YJ, Hayward BE, Parmar R, Robins P, Leitch A, Ali M, Black DN, van Bokhoven H, Brunner HG, Hamel BC, et al. Mutations in the gene encoding the 3′–5′ DNA exonuclease TREX1 cause Aicardi-Goutieres syndrome at the AGS1 locus. Nat Genet. 2006; 38:917–920. [PubMed: 16845398]

Dauer WT, Worman HJ. The nuclear envelope as a signaling node in development and disease. Dev Cell. 2009; 17:626–638. [PubMed: 19922868]

Delgado-Vega AM, Alarcon-Riquelme ME, Kozyrev SV. Genetic associations in type I interferon related pathways with autoimmunity. Arthritis Res Ther. 2010; 12(Suppl 1):S2. [PubMed: 20392289]

Drake KR, Kang M, Kenworthy AK. Nucleocytoplasmic distribution and dynamics of the autophagosome marker EGFP-LC3. PLoS One. 2010; 5:e9806. [PubMed: 20352102]

Evans CJ, Aguilera RJ. DNase II: genes, enzymes and function. Gene. 2003; 322:1–15. [PubMed: 14644493]

Ferguson BJ, Mansur DS, Peters NE, Ren H, Smith GL. DNA-PK is a DNA sensor for IRF-3-dependent innate immunity. Elife. 2012; 1:e00047. [PubMed: 23251783]

Gall A, Treuting P, Elkon KB, Loo YM, Gale M Jr, Barber GN, Stetson DB. Autoimmunity Initiates in Nonhematopoietic Cells and Progresses via Lymphocytes in an Interferon-Dependent Autoimmune Disease. Immunity. 2012; 36:120–131. [PubMed: 22284419]

Galluzzi L, Senovilla L, Zitvogel L, Kroemer G. The secret ally: immunostimulation by anticancer drugs. Nat Rev Drug Discov. 2012; 11:215–233. [PubMed: 22301798]

Gomez M, Antequera F. Overreplication of short DNA regions during S phase in human cells. Genes Dev. 2008; 22:375–385. [PubMed: 18245449]

Graham RR, Hom G, Ortmann W, Behrens TW. Review of recent genome-wide association scans in lupus. J Intern Med. 2009; 265:680–688. [PubMed: 19493061]

Green BM, Finn KJ, Li JJ. Loss of DNA replication control is a potent inducer of gene amplification. Science. 2010; 329:943–946. [PubMed: 20724634]

Hande MP, Balajee AS, Tchirkov A, Wynshaw-Boris A, Lansdorp PM. Extra-chromosomal telomeric DNA in cells from Atm(−/−) mice and patients with ataxia-telangiectasia. Hum Mol Genet. 2001; 10:519–528. [PubMed: 11181576]

Hasan M, Koch J, Rakheja D, Pattnaik AK, Brugarolas J, Dozmorov I, Levine B, Wakeland EK, Lee-Kirsch MA, Yan N. Trex1 regulates lysosomal biogenesis and interferon-independent activation of antiviral genes. Nat Immunol. 2013; 14:61–71. [PubMed: 23160154]

Hinz M, Stilmann M, Arslan SC, Khanna KK, Dittmar G, Scheidereit C. A cytoplasmic ATM-TRAF6-cIAP1 module links nuclear DNA damage signaling to ubiquitin-mediated NF-kappaB activation. Mol Cell. 2010; 40:63–74. [PubMed: 20932475]

Ikegami S, Taguchi T, Ohashi M, Oguro M, Nagano H, Mano Y. Aphidicolin prevents mitotic cell division by interfering with the activity of DNA polymerase-alpha. Nature. 1978; 275:458–460. [PubMed: 692726]

Ishii KJ, Akira S. Innate immune recognition of, and regulation by, DNA. Trends Immunol. 2006; 27:525–532. [PubMed: 16979939]

Ivanov A, Pawlikowski J, Manoharan I, van Tuyn J, Nelson DM, Rai TS, Shah PP, Hewitt G, Korolchuk VI, Passos JF, et al. Lysosome-mediated processing of chromatin in senescence. J Cell Biol. 2013; 202:129–143. [PubMed: 23816621]

Iwasaki A. A virological view of innate immune recognition. Annu Rev Microbiol. 2012; 66:177–196. [PubMed: 22994491]

Kaiser R, Criswell LA. Genetics research in systemic lupus erythematosus for clinicians: methodology, progress, and controversies. Curr Opin Rheumatol. 2010; 22:119–125. [PubMed: 20035223]

Kanda T, Sullivan KF, Wahl GM. Histone-GFP fusion protein enables sensitive analysis of chromosome dynamics in living mammalian cells. Curr Biol. 1998; 8:377–385. [PubMed: 9545195]

Kawane K, Fukuyama H, Kondoh G, Takeda J, Ohsawa Y, Uchiyama Y, Nagata S. Requirement of DNase II for definitive erythropoiesis in the mouse fetal liver. Science. 2001; 292:1546–1549. [PubMed: 11375492]

Kawane K, Ohtani M, Miwa K, Kizawa T, Kanbara Y, Yoshioka Y, Yoshikawa H, Nagata S. Chronic polyarthritis caused by mammalian DNA that escapes from degradation in macrophages. Nature. 2006; 443:998–1002. [PubMed: 17066036]

Kawane K, Tanaka H, Kitahara Y, Shimaoka S, Nagata S. Cytokine-dependent but acquired immunity-independent arthritis caused by DNA escaped from degradation. Proc Natl Acad Sci U S A. 2010; 107:19432–19437. [PubMed: 20974942]

Kawashima A, Tanigawa K, Akama T, Wu H, Sue M, Yoshihara A, Ishido Y, Kobiyama K, Takeshita F, Ishii KJ, et al. Fragments of genomic DNA released by injured cells activate innate immunity and suppress endocrine function in the thyroid. Endocrinology. 2011; 152:1702–1712. [PubMed: 21303947]

Ko A, Kanehisa A, Martins I, Senovilla L, Chargari C, Dugue D, Marino G, Kepp O, Michaud M, Perfettini JL, et al. Autophagy inhibition radiosensitizes in vitro, yet reduces radioresponses in vivo due to deficient immunogenic signalling. Cell Death Differ. 2014; 21:92–99. [PubMed: 24037090]

Kobiyama K, Takeshita F, Jounai N, Sakaue-Sawano A, Miyawaki A, Ishii KJ, Kawai T, Sasaki S, Hirano H, Ishii N, et al. Extra chromosomal histone H2B mediates innate antiviral immune responses induced by intracellular double-stranded DNA. J Virol. 2010; 84:822–832. [PubMed: 19906922]

Kondo T, Kobayashi J, Saitoh T, Maruyama K, Ishii KJ, Barber GN, Komatsu K, Akira S, Kawai T. DNA damage sensor MRE11 recognizes cytosolic double-stranded DNA and induces type I interferon by regulating STING trafficking. Proc Natl Acad Sci U S A. 2013; 110:2969–2974. [PubMed: 23388631]

Krick R, Muehe Y, Prick T, Bremer S, Schlotterhose P, Eskelinen EL, Millen J, Goldfarb DS, Thumm M. Piecemeal microautophagy of the nucleus requires the core macroautophagy genes. Mol Biol Cell. 2008; 19:4492–4505. [PubMed: 18701704]

Krieser RJ, MacLea KS, Longnecker DS, Fields JL, Fiering S, Eastman A. Deoxyribonuclease IIalpha is required during the phagocytic phase of apoptosis and its loss causes perinatal lethality. Cell Death Differ. 2002; 9:956–962. [PubMed: 12181746]

Lee-Kirsch MA, Gong M, Chowdhury D, Senenko L, Engel K, Lee YA, de Silva U, Bailey SL, Witte T, Vyse TJ, et al. Mutations in the gene encoding the 3′-5′ DNA exonuclease TREX1 are associated with systemic lupus erythematosus. Nat Genet. 2007; 39:1065–1067. [PubMed: 17660818]

Mazur DJ, Perrino FW. Excision of 3′ termini by the Trex1 and TREX2 3′-->5′ exonucleases. Characterization of the recombinant proteins. J Biol Chem. 2001; 276:17022–17029. [PubMed: 11279105]

Mijaljica D, Prescott M, Devenish RJ. The intricacy of nuclear membrane dynamics during nucleophagy. Nucleus. 2010; 1:213–223. [PubMed: 21327066]

Morita M, Stamp G, Robins P, Dulic A, Rosewell I, Hrivnak G, Daly G, Lindahl T, Barnes DE. Gene-targeted mice lacking the Trex1 (DNase III) 3′-->5′ DNA exonuclease develop inflammatory myocarditis. Mol Cell Biol. 2004; 24:6719–6727. [PubMed: 15254239]

Nagai S, Dubrana K, Tsai-Pflugfelder M, Davidson MB, Roberts TM, Brown GW, Varela E, Hediger F, Gasser SM, Krogan NJ. Functional targeting of DNA damage to a nuclear pore-associated SUMO-dependent ubiquitin ligase. Science. 2008; 322:597–602. [PubMed: 18948542]

Napirei M, Karsunky H, Zevnik B, Stephan H, Mannherz HG, Moroy T. Features of systemic lupus erythematosus in Dnase1-deficient mice. Nat Genet. 2000; 25:177–181. [PubMed: 10835632]

Novakova Z, Hubackova S, Kosar M, Janderova-Rossmeislova L, Dobrovolna J, Vasicova P, Vancurova M, Horejsi Z, Hozak P, Bartek J, et al. Cytokine expression and signaling in drug-induced cellular senescence. Oncogene. 2010; 29:273–284. [PubMed: 19802007]

Oza P, Jaspersen SL, Miele A, Dekker J, Peterson CL. Mechanisms that regulate localization of a DNA double-strand break to the nuclear periphery. Genes Dev. 2009; 23:912–927. [PubMed: 19390086]

Ozeri-Galai E, Bester AC, Kerem B. The complex basis underlying common fragile site instability in cancer. Trends Genet. 2012; 28:295–302. [PubMed: 22465609]

Paludan SR, Bowie AG. Immune sensing of DNA. Immunity. 2013; 38:870–880. [PubMed: 23706668]

Pang D, Winters TA, Jung M, Purkayastha S, Cavalli LR, Chasovkikh S, Haddad BR, Dritschilo A. Radiation-generated short DNA fragments may perturb non-homologous end-joining and induce genomic instability. J Radiat Res (Tokyo). 2011; 52:309–319. [PubMed: 21628845]

Park JS, Lim MA, Cho ML, Ryu JG, Moon YM, Jhun JY, Byun JK, Kim EK, Hwang SY, Ju JH, et al. p53 controls autoimmune arthritis via STAT-mediated regulation of the Th17 cell/Treg cell balance in mice. Arthritis Rheum. 2013; 65:949–959. [PubMed: 23280308]

Park YE, Hayashi YK, Bonne G, Arimura T, Noguchi S, Nonaka I, Nishino I. Autophagic degradation of nuclear components in mammalian cells. Autophagy. 2009; 5:795–804. [PubMed: 19550147]

Rello-Varona S, Lissa D, Shen S, Niso-Santano M, Senovilla L, Marino G, Vitale I, Jemaa M, Harper F, Pierron G, et al. Autophagic removal of micronuclei. Cell Cycle. 2012; 11:170–176. [PubMed: 22185757]

Robert T, Vanoli F, Chiolo I, Shubassi G, Bernstein KA, Rothstein R, Botrugno OA, Parazzoli D, Oldani A, Minucci S, et al. HDACs link the DNA damage response, processing of double-strand breaks and autophagy. Nature. 2011; 471:74–79. [PubMed: 21368826]

Roberts P, Moshitch-Moshkovitz S, Kvam E, O'Toole E, Winey M, Goldfarb DS. Piecemeal microautophagy of nucleus in Saccharomyces cerevisiae. Mol Biol Cell. 2003; 14:129–141. [PubMed: 12529432]

Saitoh T, Fujita N, Hayashi T, Takahara K, Satoh T, Lee H, Matsunaga K, Kageyama S, Omori H, Noda T, et al. Atg9a controls dsDNA-driven dynamic translocation of STING and the innate immune response. Proc Natl Acad Sci U S A. 2009; 106:20842–20846. [PubMed: 19926846]

Settembre C, Fraldi A, Jahreiss L, Spampanato C, Venturi C, Medina D, de Pablo R, Tacchetti C, Rubinsztein DC, Ballabio A. A block of autophagy in lysosomal storage disorders. Hum Mol Genet. 2008; 17:119–129. [PubMed: 17913701]

Shoji JY, Kikuma T, Arioka M, Kitamoto K. Macroautophagy-mediated degradation of whole nuclei in the filamentous fungus Aspergillus oryzae. PLoS One. 2010; 5:e15650. [PubMed: 21187926]

Sogo JM, Lopes M, Foiani M. Fork reversal and ssDNA accumulation at stalled replication forks owing to checkpoint defects. Science. 2002; 297:599–602. [PubMed: 12142537]

Stetson DB, Ko JS, Heidmann T, Medzhitov R. Trex1 prevents cell-intrinsic initiation of autoimmunity. Cell. 2008; 134:587–598. [PubMed: 18724932]

Stetson DB, Medzhitov R. Recognition of cytosolic DNA activates an IRF3-dependent innate immune response. Immunity. 2006; 24:93–103. [PubMed: 16413926]

Sugihara T, Murano H, Nakamura M, Ichinohe K, Tanaka K. Activation of interferon-stimulated genes by gamma-ray irradiation independently of the ataxia telangiectasia mutated-p53 pathway. Mol Cancer Res. 2011; 9:476–484. [PubMed: 21357441]

Watson RO, Manzanillo PS, Cox JS. Extracellular M. tuberculosis DNA targets bacteria for autophagy by activating the host DNA-sensing pathway. Cell. 2012; 150:803–815. [PubMed: 22901810]

Yang Y, Xia F, Hermance N, Mabb A, Simonson S, Morrissey S, Gandhi P, Munson M, Miyamoto S, Kelliher MA. A cytosolic ATM/NEMO/RIP1 complex recruits TAK1 to mediate the NF-kappaB and p38 mitogen-activated protein kinase (MAPK)/MAPK-activated protein 2 responses to DNA damage. Mol Cell Biol. 2011; 31:2774–2786. [PubMed: 21606198]

Yang YG, Lindahl T, Barnes DE. Trex1 exonuclease degrades ssDNA to prevent chronic checkpoint activation and autoimmune disease. Cell. 2007; 131:873–886. [PubMed: 18045533]

Yasutomo K, Horiuchi T, Kagami S, Tsukamoto H, Hashimura C, Urushihara M, Kuroda Y. Mutation of DNASE1 in people with systemic lupus erythematosus. Nat Genet. 2001; 28:313–314. [PubMed: 11479590]

Yoshida H, Okabe Y, Kawane K, Fukuyama H, Nagata S. Lethal anemia caused by interferon-beta produced in mouse embryos carrying undigested DNA. Nat Immunol. 2005; 6:49–56. [PubMed: 15568025]

Zhang X, Brann TW, Zhou M, Yang J, Oguariri RM, Lidie KB, Imamichi H, Huang DW, Lempicki RA, Baseler MW, et al. Cutting edge: Ku70 is a novel cytosolic DNA sensor that induces type III rather than type I IFN. J Immunol. 2011; 186:4541–4545. [PubMed: 21398614]

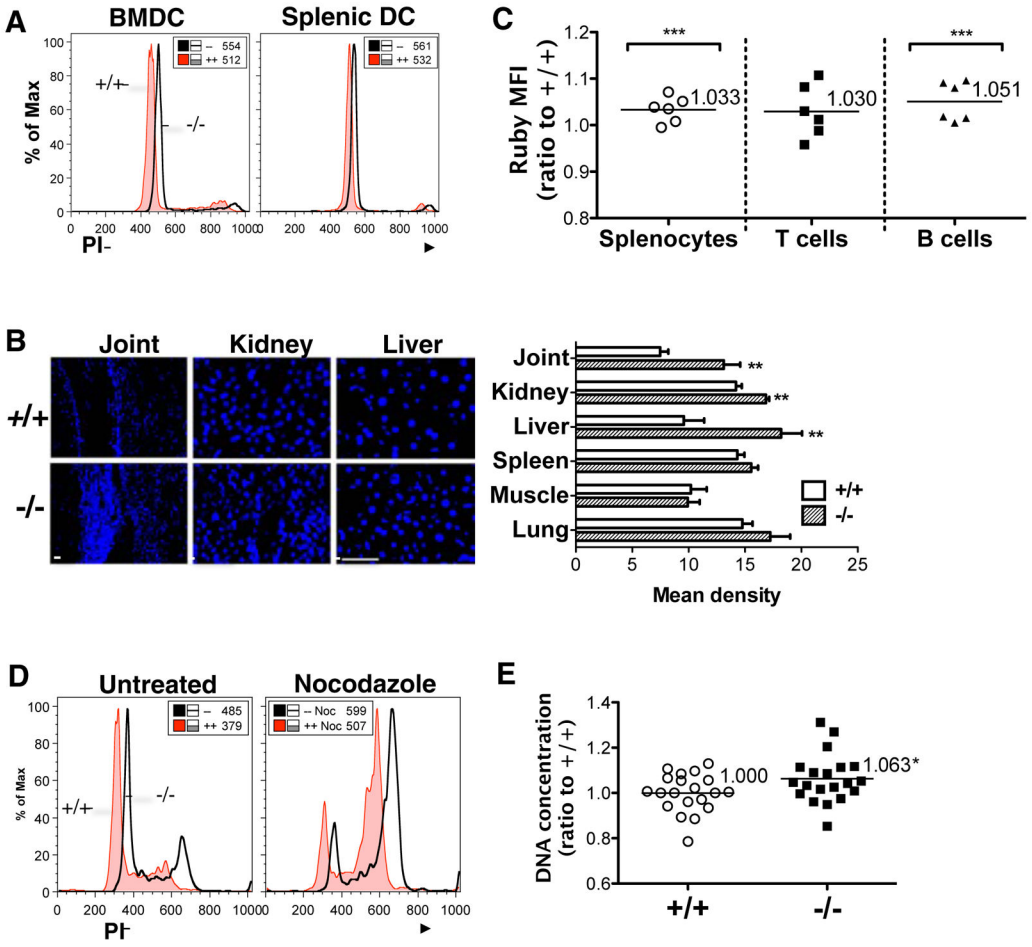


**Figure 1. Accumulation of DNA in *Dnase2a*-deficient cells**

(A) DNA content of BMDCs and splenic DCs from wild-type and *Dnase2a*$^{-/-}$ mice examined by PI staining (MFI shown), representative of 3 independent experiments with MFI ratio of *Dnase2a*$^{-/-}$ to *Dnase2a*$^{+/+}$ of 1.15±0.13 SD (BMDCs) and 1.19±0.24 SD (splenic DCs).

(B) DAPI staining of tissues from wild-type and *Dnase2a*-deficient mice. Mean density of DAPI-positive areas is based on 5–10 total fields from 2 independent comparisons of matched wild-type and knockout mice, values are mean±sem; scale bar 10 μm.

(C) Overall DNA content of live immune cells from spleens of wild-type and *Dnase2a*-deficient mice assessed by flow cytometry using Ruby dye. Each symbol represents the ratio of the MFI from cells of *Dnase2a*$^{-/-}$ vs. matched *Dnase2a*$^{+/+}$ mice. Six independent experiments were analyzed using a regression model to account for technical batch effect and biological variation; mean MFI ratios for all experiments per cell type are indicated next to the horizontal bars that mark the mean.

(D) DNA content of nocodazole-synchronized (100 ng/ml for 16 h) *Dnase2a*$^{+/+}$ and *Dnase2a*$^{-/-}$ MLFs by PI staining, representative of 3 independent experiments with MFI shown, $p<0.05$.

(E) Relative amount of purified genomic DNA content from *Dnase2a*$^{+/+}$ or *Dnase2a*$^{-/-}$ MLFs by UV absorbance. Each data point is the ratio of DNA from a single sample vs. the mean of all *Dnase2a*$^{+/+}$ samples. Horizontal bars mark mean ratios.
See also Figure S1.

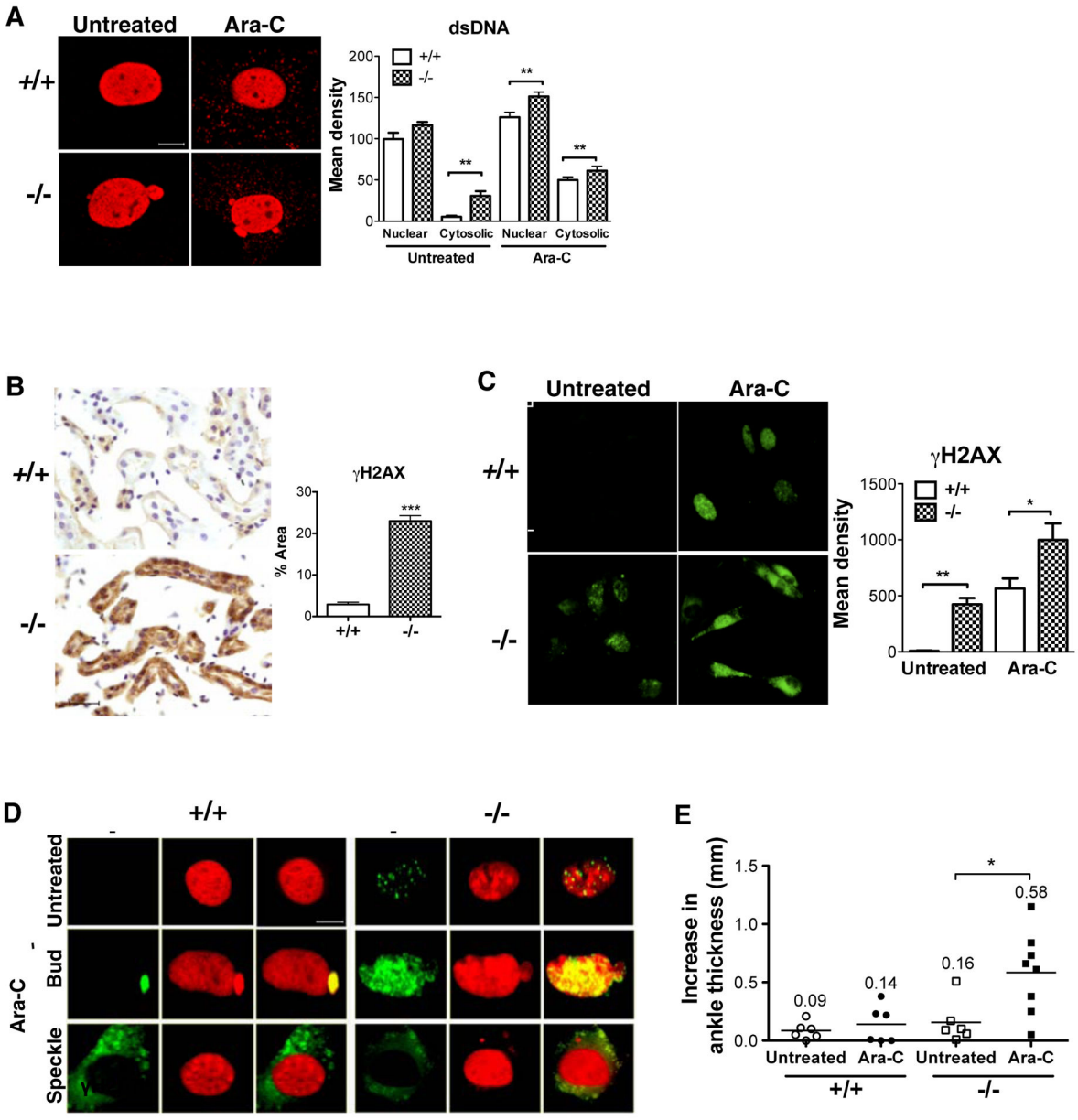


**Figure 2. Damaged DNA in the cytosol of *Dnase2a*-deficient cells**

(A) Fluorescent staining of MLFs from wild-type or *Dnase2a*$^{-/-}$ mice with anti-dsDNA antibodies; scale bar, 10 μm. Right panel, quantitation of dsDNA in nuclear and cytosolic compartments based on 5 total fields of 20X from 3 independent experiments.

(B) Immunoperoxidase staining of anti-γ-H2AX in kidneys of wild-type and *Dnase2a*$^{-/-}$ mice, scale bar, 10 μm; right panel, quantitation of signals as % total area based on 5 fields of 20X from 3 matched pairs of wild-type and *Dnase2a*$^{-/-}$ mice.

(C) Immunofluorescent staining of anti-γ-H2AX in MLFs, scale bar, 50 μm; right panel, quantitation of signals as mean density based on 5 fields of 20X from 3 independent experiments.

(D) Double-staining with anti-γ-H2AX (green) and anti-dsDNA (red) antibodies in MLFs; yellow indicates co-localization; scale bar, 10 μm; images representative of 3 independent experiments.

(E) Increase in ankle thickness from week 0 to week 8 (for both ankles) in matched 10–12 weeks old wild-type and *Dnase2a*$^{-/-}$ mice (n=3–4), untreated or injected with 3 doses of 15 μg/g Ara-C *i.p.*, mean increase is shown numerically.

See also Figure S2.

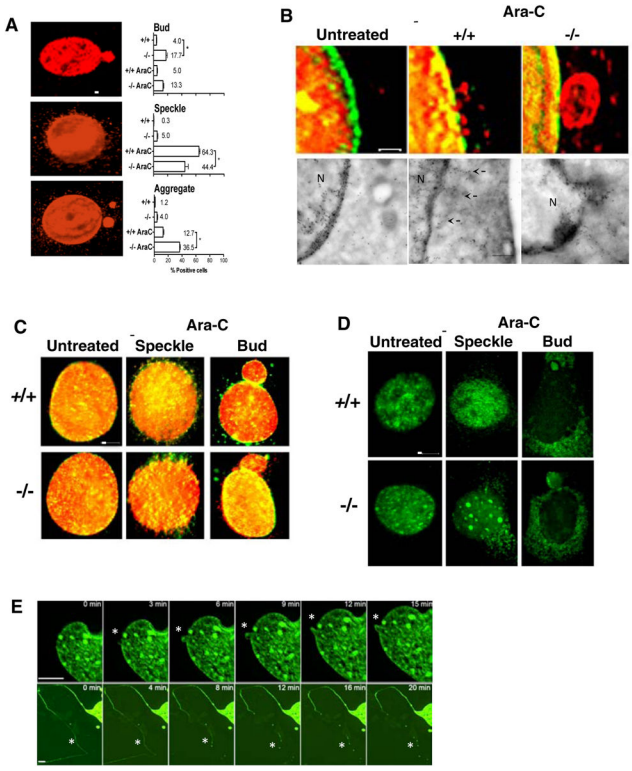


**Figure 3. Export of DNA from nucleus to cytosol**

(A) Left panel, immunostaining of anti-dsDNA shows three distinct extra-nuclear DNA patterns quantified in MLFs: nuclear buds, cytosolic speckles, large extra-nuclear aggregates; scale bar, 10 μm. Right panel, frequencies in *Dnase2a*$^{+/+}$ and *Dnase2a*$^{-/-}$ MLFs, without or with Ara-C treatment (10 μM, 24 h), based on 10 fields at 20X. Frequency of normal nuclei is not shown.

(B) Representative images of immunofluorescence staining (anti-NUP98, green; anti-dsDNA, red; scale bar, 2 μm) and electron microscopy (immuno-gold anti-dsDNA antibodies; scale bar, 500 nm; N, nucleus) in MLFs. Untreated cell with clear cytoplasm is a *Dnase2a*$^{+/+}$ MLF.

(C) Anti-dsDNA (red) and anti-NUP98 (green) staining in MLFs; scale bar, 10 μm.

(D) MLFs pulsed with BrdU (15 μM for 6 h) show newly replicated DNA in buds and speckles; scale bar, 10 μm.

(E) Sequences from time-lapse imaging of GFP-H2B-infected MLFs illustrating nuclear DNA budding (top series) and thread formation/detachment (bottom series); scale bar, 5 μm; asterisks highlight changes.

See also Figure S3, Video 1, 2.

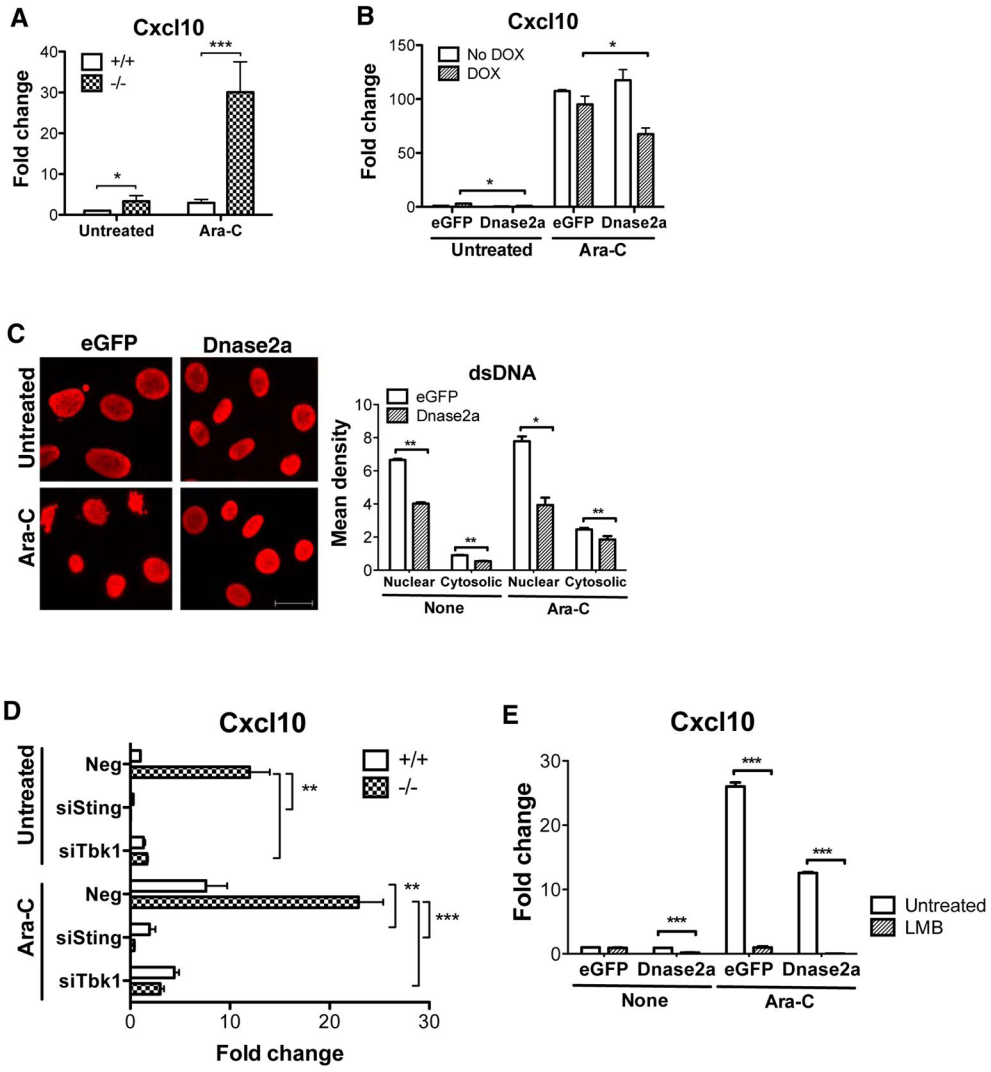


**Figure 4. Accumulated DNA activates Sting-dependent inflammation**

(A) Expression of *Cxcl10* mRNA in untreated or Ara-C treated wild-type and Dnase2a$^{-/-}$ MLFs.

(B) *Cxcl10* expression of *Dnase2a*$^{-/-}$ MLFs rescued with *Dnase2a* ORF using a Tet-on vector with doxycycline induction (3 μg/ml, 24 h); *eGFP* ORF was used as negative control.

(C) Immunostaining of anti-dsDNA for KO and rescued cells (as in B); scale bar, 20 μm; right panel, quantitation of fluorescent signals based on 5 fields of 20X.

(D) *Cxcl10* mRNA levels in *Dnase2a*$^{+/+}$ and *Dnase2a*$^{-/-}$ MLFs transfected with siRNAs targeting *Sting* or *Tbk1*, untreated or treated with 10 μM Ara-C for 24 h.

(E) *Cxcl10* expression of KO or rescued MLFs after doxycycline induction, untreated or treated with Ara-C and leptomycin (20 nM, 24 h) as indicated. Data are representative of two (B, C, D) or three (A, E) independent experiments.

See also Figure S4.

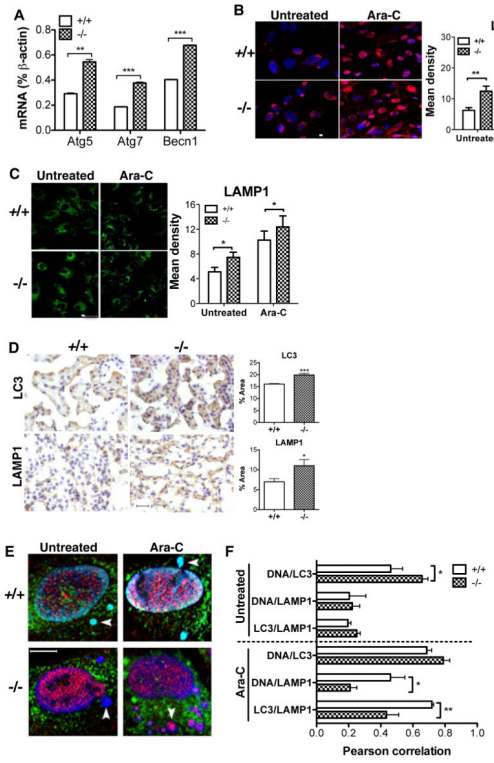


**Figure 5. Autophagy in *Dnase2a* deficiency**

(A) Levels of autophagy gene mRNAs in wild type and *Dnase2a*$^{-/-}$ MLFs.

(B) Immunostaining with anti-LC3 antibodies (red) in *Dnase2a*$^{+/+}$ and *Dnase2a*$^{-/-}$ MLFs showing punctate patterns, DAPI (blue) as counter-stain; scale bar, 10 μm; right panel, quantitation of LC3 signal.

(C) Immunostaining with anti-LAMP1 antibodies in *Dnase2a*$^{+/+}$ and *Dnase2a*$^{-/-}$ MLFs; scale bar, 10 μm; right panel, quantitation of LAMP1 signal.

(D) Expression of LC3 and LAMP1 in kidneys of wild-type and *Dnase2a*$^{-/-}$ mice by immunoperoxidase detection and counter-stained by hematoxylin, scale bar, 10 μm; quantitation in % total area based on 6 random fields at 20X.

(E) Three-color confocal staining with anti-dsDNA (blue), anti-LC3 (red) and anti-LAMP1 (green) antibodies in wild-type and *Dnase2a*$^{-/-}$ MLFs (arrowheads indicate extra-nuclear DNA aggregates); scale bar, 10 μm.

(F) Quantitation of overlap between pairs of stains (from experiment in E). Quantitation of fluorescent signals in B, C and E is based on 5–10 fields at 20X of duplicate experiments. See also Figure S5.

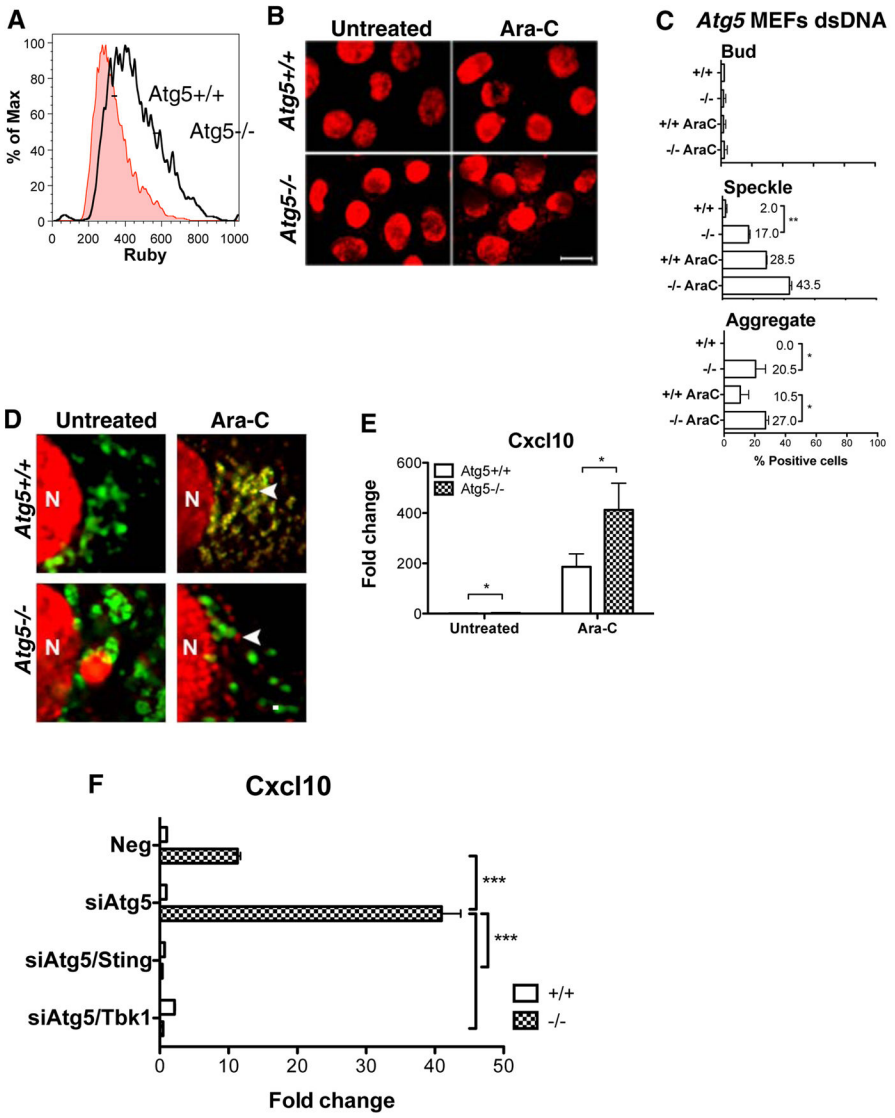


**Figure 6. Role of autophagy and lysosomes in autonomous DNA removal**

(A) DNA content of *Atg5*$^{+/+}$ and *Atg5*$^{-/-}$ MEFs by Ruby staining.

(B) Immunostaining of anti-dsDNA in *Atg5*$^{+/+}$ vs. *Atg5*$^{-/-}$ MEFs with or without Ara-C treatment; scale bar, 20 μm.

(C) Relative frequencies of bud, speckle and aggregate patterns in *Atg5*$^{+/+}$ and *Atg5*$^{-/-}$ MEFs.

(D) Anti-LAMP1 (green) and anti-dsDNA (red) dual staining in *Atg5*$^{-/-}$ MEFs vs. *Atg5*$^{+/+}$ cells, scale bar, 2 μm; N denotes nucleus.

(E) Ratio of *Cxcl10* mRNA levels in *Atg5*$^{+/+}$ vs. *Atg5*$^{-/-}$ MEFs with or without Ara-C treatment.

(F) Relative *Cxcl10* expression in wild-type or *Dnase2a*$^{-/-}$ MLFs silenced with siRNAs.

All data are results of independent duplicate experiments.

See also Figure S6.